PROCEEDINGS OF SCIENCE

Effects of Biaxial Birefringence on Polarization Reconstruction for the Askaryan Radio Array

Alan Salcedo-Gomez,[a,*] **Justin Flaherty**[a] **and Amy Connolly**[a] **for the ARA Collaboration**

(a complete list of authors can be found at the end of the proceedings)

[a] *The Ohio State University,*
281 W Lane Ave, Columbus, OH, United States

E-mail: salcedogomez.1@osu.edu

Ultra-high energy (UHE) neutrinos, with energies exceeding 10^{17} eV, offer unique insights into cosmic accelerators and the origins of ultra-high energy cosmic rays. The Askaryan Radio Array (ARA) is designed to detect UHE neutrinos by capturing radio signals generated by their interactions within Antarctic ice. Observations from the South Pole Ice Core Experiment (SPICE) pulsing campaign revealed unexpected polarization effects in detected radio pulses transmitted through polar ice. This paper explores the impact of biaxial birefringence in South Pole ice on the polarization of SPICE pulses. We present a model that accounts for biaxial birefringence effects, showing how signal polarization can rotate during propagation through the ice. We show that the biaxial birefringence model can potentially explain the unexpected polarization results observed in SPICE data and highlight the need to validate the model to enhance future analyses and detector designs.

10th International Workshop on Acoustic and Radio EeV Neutrino Detection Activities (ARENA2024)
11-14 June 2024
The Kavli Institute for Cosmological Physics, Chicago, IL, USA

*Speaker

PoS(ARENA2024)009

1. Introduction

Ultra-high energy (UHE) neutrinos ($E_\nu \geq 10^{17}$ eV) are a decisive missing piece in the field of multi-messenger astrophysics. Recent achievements in this field include the discovery of a high-energy astrophysical neutrino flux reaching up to 10 PeV, the first detection of gravitational waves, and the precise measurement of cosmic rays and gamma rays at their largest detectable energy limits [1, 2]. UHE neutrinos could reveal the nature of cosmic accelerators that generate cosmic rays exceeding 10^{20} eV.

UHE neutrinos likely originate from both astrophysical sources through hadronic processes and from interactions like the Greisen-Zatsepin-Kuzmin (GZK) effect, where extragalactic cosmic rays with energies above $10^{19.5}$ eV interact with the cosmic microwave background within tens of Mpc of their origin [3, 4]. Therefore, these neutrinos would point close to the cosmic ray production site. Unlike cosmic rays and high-energy photons, neutrinos are not deflected or absorbed, making them ideal for tracing the most energetic cosmic accelerators.

When neutrinos interact in a dense medium like ice, they produce a radio pulse through the Askaryan effect, a form of coherent Cherenkov radiation at radio frequencies [5, 6]. Experiments such as the Askaryan Radio Array (ARA) shown in Figure 1, use radio antennas at polar ice sheets to detect these signals [7–9]. Since radio waves can travel distances of kilometers in ice due to their long attenuation length, understanding ice effects on signal propagation over these distance scales is crucial. In particular, analyzing signal polarization is essential for determining the incoming direction of UHE neutrinos and identifying their sources.

In this paper, we first describe the South Pole Ice Core Experiment (SPICE) and its role in studying radio signal propagation in ice (Section 2). We then discuss biaxial birefringence in South Pole ice (Section 3). Following this, we present a model for biaxial birefringence applied to ARA and compare simulated results with experimental data (Section 4). Finally, we discuss our findings and implications for UHE neutrino detection and future research (Section 5).

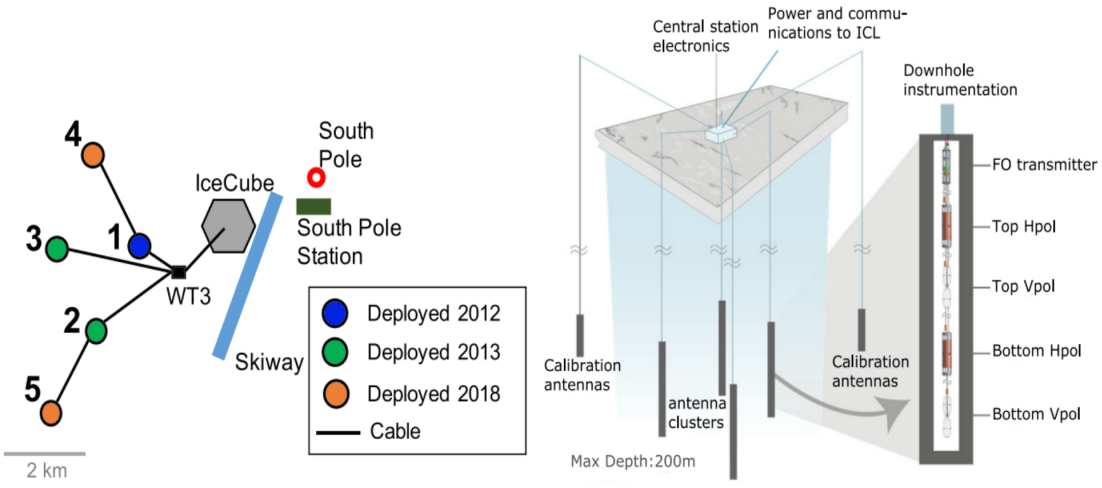

Figure 1: (Left) Layout of ARA array relative to IceCube and the South Pole. (Right) Layout of an ARA station. FO is a fiber-optic transmitter.

2. The South Pole Ice Core Experiment

The South Pole Ice Core Experiment (SPICE) calibration system enabled the study of radio signals propagating kilometer-scale distances by generating a unique dataset of impulsive signals with both transmitters and receivers embedded within the ice. As depicted in Figure 2, the ARA and ARIANNA in-ice neutrino experiments detected SPICE radiofrequency impulses as far as 4 km away. Five ARA stations (A1-A5) recorded these pulses at depths of 100 to 200 meters, while two ARIANNA stations detected them just below the surface.

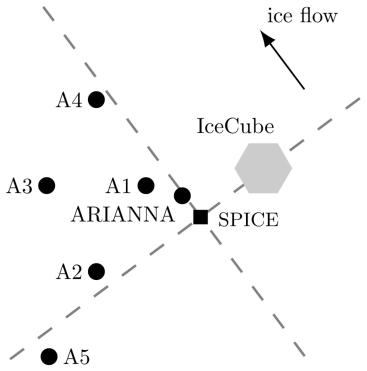

Figure 2: Layout of SPICE, the five ARA stations, the ARIANNA South Pole station, and IceCube.

Both ARA and ARIANNA observed unexpected polarization effects in the SPICE pulses. Although the SPICE pulses were primarily transmitted with vertical polarization (Vpol), they often exhibited greater-than-expected power in the horizontal polarization (Hpol), and in some cases, the horizontal polarization showed more power than the original polarization. Additionally, the relationship between the observed signal polarization and the receiver positions did not follow consistent patters [10, 11].

3. Biaxial Birefringence

3.1 Electromagnetism in biaxal birefringent crystals

Birefringent crystals are anisotropic media where the propagation of electromagnetic radiation depends on its direction and polarization due to properties of one or more axes within the crystal. A biaxial birefringent crystal has symmetry about two axes and is characterized by three parameters measured along three perpendicular directions. South Pole ice is believed to behave as a biaxially birefringent medium at radio frequencies, influenced by two key axes: 1) the vertical axis, shaped by compression, and 2) the horizontal plane, shaped by the direction of ice flow [12].

In a biaxially birefringent crystal, a wave vector $\mathbf{k}$ produces not just one, but two distinct rays, each traveling with a different refractive index. These rays are associated with polarization —or displacement— eigenvectors $\mathbf{D_1}$ and $\mathbf{D_2}$, such that $\mathbf{D_1} \times \mathbf{D_2} = \mathbf{k}$. To determine $\mathbf{D_1}$ and $\mathbf{D_2}$, we consider the three medium parameters, called principal axes: n_α, n_β, and n_γ. These parameters, which vary with depth at the South Pole (see Figure 3), define the three perpendicular semi-axes of an ellipsoid known as the "indicatrix", with the α-axis aligned with ice flow and the γ-axis with

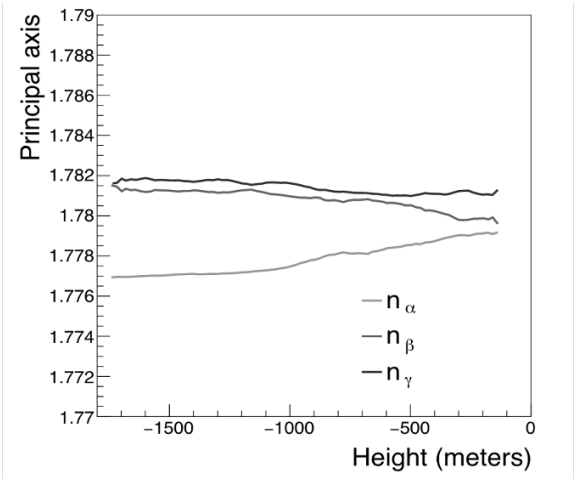

Figure 3: Principal axes reported by Voigt [13] and used by Connolly [12]

compression. The intersection of the signal's wavefront, perpendicular to **k**, with the indicatrix forms an ellipse. The directions of $\mathbf{D_1}$ and $\mathbf{D_2}$ align with the major and minor axes of this ellipse, and the lengths of these axes correspond to the refractive indices experienced by the two rays. This is illustrated in Figure 4, where the $\mathbf{D_1}$ and $\mathbf{D_2}$ are aligned with 3 o'clock and 12 o'clock, respectively. The 12 o'clock direction is perpendicular to **k** and in the plane of **k** and the γ-axis.

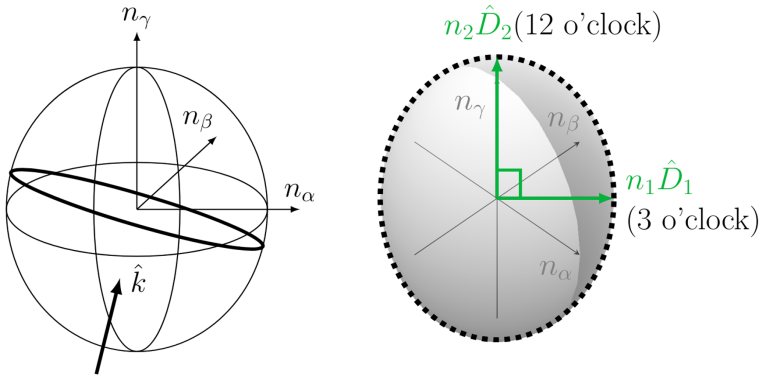

Figure 4: (Left) Illustration of an indicatrix. We show an ellipse representing the intersection of a wavefront and its wave vector **k** with the indicatrix. (Right) Example of an intersection ellipse with $\mathbf{D_1}$ and $\mathbf{D_2}$ aligned along 3 o'clock and 12 o'clock, respectively.

3.2 Modeling biaxial birefringence for ARA

The direction of propagation and refractive index of radio signals change as they travel. To account for this, we divide the propagation into N small incremental steps, assuming these quantities are constant within each step. We calculate the signal trajectory without considering birefringence effects. The time delay between eigenstates $\mathbf{D_1}$ and $\mathbf{D_2}$ at the receiver position is given by

$$T = \sum_{i=1}^{N} \frac{\Delta l_i}{c}(n_{2i} - n_{1i}) \tag{1}$$

where c is the speed of light in vacuum, Δl_i denotes the distance between the points i and $i-1$ along the ray path, and n_{1i} and n_{2i} are the refractive indices experienced by $\mathbf{D_1}$ and $\mathbf{D_2}$ at point i, respectively. In this model, we assume that the polarization eigenvectors change direction adiabatically due to gradual variations in the local indicatrix $(n_\alpha(z), n_\beta(z), n_\gamma(z))$ and the direction of $\mathbf{k}$. As a result, the polarization angle of a radio signal Ψ, measured from 12 o'clock, rotates as the signal travels from the transmitter (Tx) to the receiver (Rx). This process is conceptually illustrated in Figure 5.

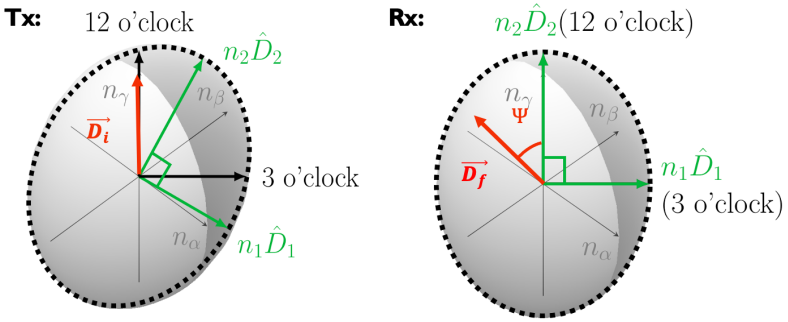

Figure 5: Illustration of the initial polarization vector $\mathbf{D_i}$ rotating from the transmitter to the receiver —becoming final polarization vector $\mathbf{D_f}$— and making a polarization angle Ψ from 12 o'clock.

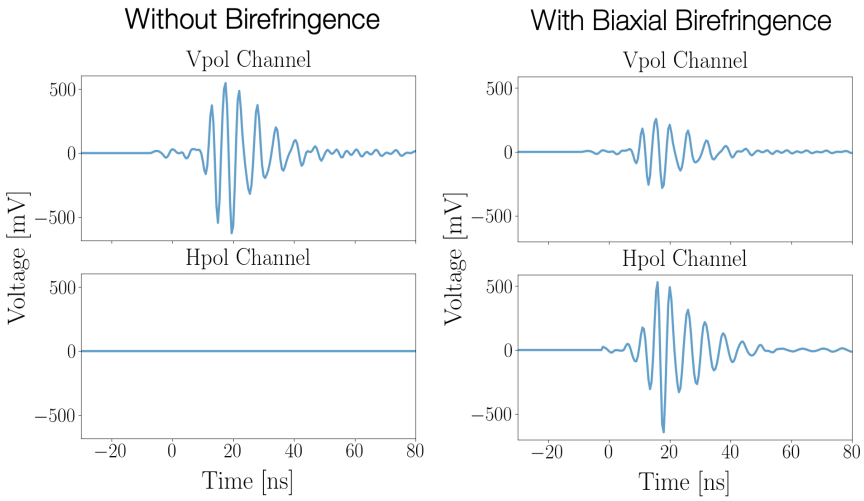

Figure 6: Simulated SPICE pulse from a depth of 1600 m detected by a pair of Vpol and Hpol channels of A4 with (right) and without (left) effects of biaxial birefringence. We subtracted ambient noise and applied channel-specific antenna and detector responses to the signals.

4. Results

4.1 The SPICE pulser polarization: simulations and data

We implemented this birefringence model in AraSim [14], which simulates signal generation, propagation and attenuation, ambient noise, and the response of the ARA detectors. We simulated

pulser signals transmitted from SPICE to ARA stations A2 and A4. Station A2 is aligned perpendicular to the ice flow, while station A4 is parallel, representing the two directions of interest. Figure 6 displays waveforms of simulated pulses emitted from SPICE at a depth of 1600 m and detected by antennas (channels) of A4 sensitive to Vpol and Hpol. Here, Vpol and Hpol signals correspond to **D** aligned with 12 o'clock and 3 o'clock, respectively. These simulated pulses are emitted with vertical polarization and are detected only the Vpol channels when biaxial birefringence is not considered. However, including biaxial birefringence effects results in detection by Hpol channels, indicating signal rotation.

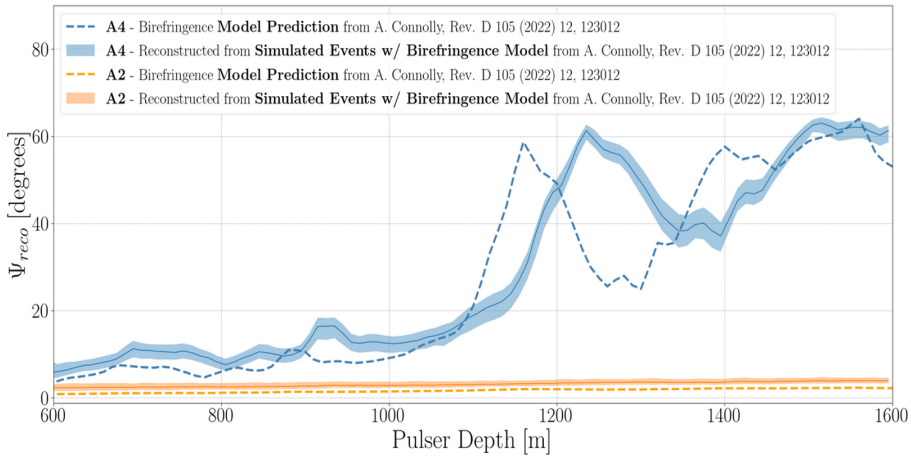

Figure 7: Comparison of predicted (dashed lines) and simulated (solid-banded lines) polarization angles Ψ_{reco} as a function of depth for SPICE pulses detected by A2 (orange) and A4 (blue). The bands around solid lines represent 1σ statistical uncertainties in polarization reconstruction due to noise in the waveforms.

To test our model implementation, we compared model predictions to simulated polarization angles Ψ as a function of depth for SPICE pulses detected by A2 and A4 (See Figure 7). We used the polarization reconstruction method described by Flaherty [15] on simulated waveforms. The model prediction and reconstructed polarization angle for A2 match within a systematic offset of about 4° due to noise on waveforms. This is known to occur for polarization angles $\Psi < 10°$ or $\Psi > 80°$ [15]. For A4, where the predicted polarization angles are within $10° < \Psi < 80°$ for all pulser depths, discrepancies cannot be explained by systematic noise offsets and are currently under study. Figure 8 shows preliminary results of polarization reconstruction on data from the SPICE pulsing campaign for additional comparison.

4.2 Systematic uncertainties of the model

The biaxial birefringence model used in this work assumes that the indicatrix has its γ-axis vertical and the α-axis aligned with the direction of ice flow. However, measurements from other sites suggest deviations up to or exceeding 10°, which likely also applicable at the South Pole. For example, Jordan et al. [16] found the β-axis at the North Greenland Eemian Ice Drilling (NEEM) site is up to 25° away from its expected direction perpendicular to ice flow. We denote the angle that the α-axis makes with the direction of ice flow as ϕ. Also, the tilt angles that the γ-axis makes with the vertical direction, which we will describe by θ and γ, can be obtained from either measurements of ice cores or radar measurements. For example, J. Li et al. [17] used multi-polarization radar

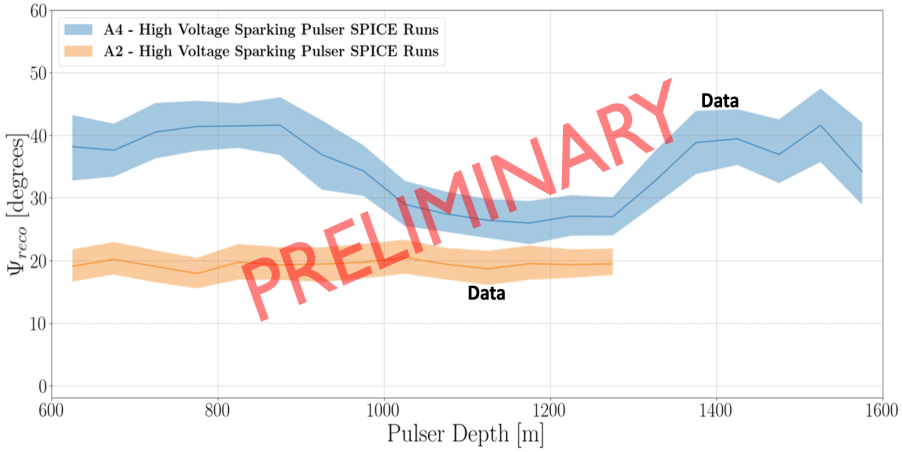

Figure 8: Preliminary results on reconstrcuted polarization angles Ψ as a function of pulser depth from runs of the High Voltage Sparking Pulser during the SPICE campaign [10].

measurements at the North Greenlad Eemian Ice Drilling (NEEM) site to ascertain a tilt angle of 9.6° from the vertical axis.

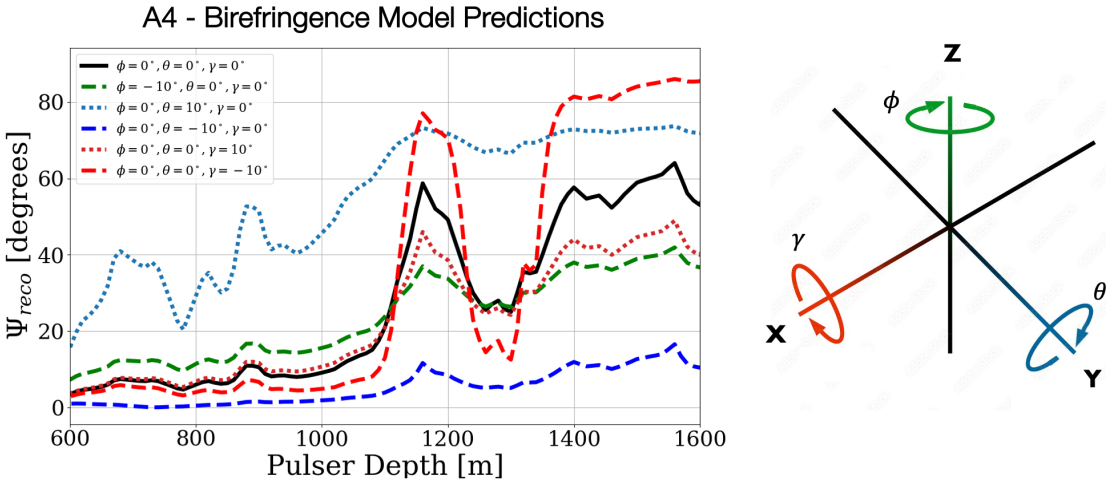

Figure 9: Model predictions of the polarization angle Ψ_{reco} as a function of depth for SPICE pulses detected by A4 assuming rotations of ±10° around the α, β, and γ-axes (x, y, and z-axes).

In Figure 9, we show model predictions for the polarization angle Ψ_{reco} for SPICE pulses detected by A4 assuming rotations of ±10° around the α, β, and γ-axes (or x, y, and z-axes, respectively). In Figure 10, we explore variations in predictions by rotating around the β-axis (or y-axis) by up to ±25°. The variations in the predictions suggest that adjusting ϕ, θ, and γ could potentially fit the qualitative shape of Ψ_{reco} observed in the SPICE data.

5. Conclusion

Biaxial birefringence of South Pole ice might explain the unexpected polarization results of the SPICE pulser. A model incorporating biaxial birefringence, based on principal axes measurements

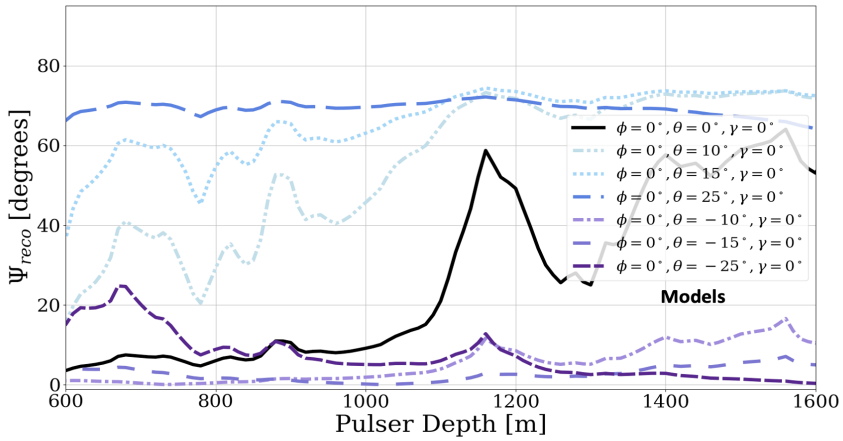

Figure 10: Model predictions of the polarization angle Ψ_{reco} as a function of depth for SPICE pulses detected by A4 by rotating around the β-axis (or y-axis) by up to ±25°.

at the SPICE location, allows for polarization rotation during signal propagation. Accurate polarization reconstruction at the neutrino interaction vertex is needed for determining the incoming direction of UHE neutrinos. The model's parameters n_α, n_β, and n_γ are reported under the assumption of perfect alignment with ice flow, cross-ice flow, and vertical directions. Rotations of ±10° around the α, β and γ axes, motivated by glaciology studies, can significantly affect polarization predictions. Furthermore, rotations of up to ±25° can lead to more significant variations, potentially allowing for the shape of Ψ_{reco} from SPICE data to be matched by fitting ϕ, θ, and γ.

Our ongoing and future work includes validating this biaxial birefringence model, using it to enable point source neutrino searches, developing new signal/background separation metrics for diffuse analyses, and optimizing antenna and detector array layouts accounting for birefringence effects. This is important for advancing UHE neutrino searches and ensuring robust astrophysical analyses upon UHE neutrino detection.

References

[1] IceCube collaboration, *Physical Review Letters* **111** (2013) .
[2] LIGO collaboration, *The Astrophysical Journal Letters* **848** (2017) L13.
[3] K. Greisen, *Phys. Rev. Lett.* **16** (1966) 748.
[4] G.T. Zatsepin and V.A. Kuzmin, *JETP Lett.* **4** (1966) 78.
[5] G.A. Askar'yan, *Zh. Eksp. Teor. Fiz.* **41** (1961) 616.
[6] D. Saltzberg et al., *Phys. Rev. Lett.* **86** (2001) 2802.
[7] ARA collaboration, *Astropart. Phys.* **35** (2012) 457.
[8] ARIANNA collaboration, *IEEE Transactions on Nuclear Science* **62** (2015) 2202.
[9] ANITA collaboration, *Astroparticle Physics* **32** (2009) 10–41.
[10] ARA collaboration, *Journal of Cosmology and Astroparticle Physics* **2020** (2020) 009–009.
[11] ARIANNA collaboration, *Journal of Instrumentation* **15** (2020) P09039–P09039.
[12] A. Connolly, *Physical Review D* **105** (2022) .
[13] D. Voigt , Technical Report , U.S. Antarctic Program (USAP) Data Center (2017).
[14] ARA collaboration, *Astroparticle Physics* **70** (2015) 62.
[15] ARA collaboration, *PoS* **ICRC2023** (2023) 1164.
[16] T.M. Jordan et al., *Annals of Glaciology* **61** (2020) 84–91.
[17] J. Li et al., *The Cryosphere* **12** (2018) 2689.

Full Author List: ARA Collaboration (July 22, 2024)

S. Ali[1], P. Allison[2], S. Archambault[3], J.J. Beatty[2], D.Z. Besson[1], A. Bishop[4], P. Chen[5], Y.C. Chen[5], Y.-C. Chen[5], B.A. Clark[6], A. Connolly[2], K. Couberly[1], L. Cremonesi[7], A. Cummings[8,9,10], P. Dasgupta[2], R. Debolt[2], S. de Kockere[11], K.D. de Vries[11], C. Deaconu[12], M. A. DuVernois[4], J. Flaherty[2], E. Friedman[6], R. Gaior[3], P. Giri[13], J. Hanson[14], N. Harty[15], K.D. Hoffman[6], M.-H. Huang[5,16], K. Hughes[2], A. Ishihara[3], A. Karle[4], J.L. Kelley[4], K.-C. Kim[6], M.-C. Kim[3], I. Kravchenko[13], R. Krebs[8,9], C.Y. Kuo[5], K. Kurusu[3], U.A. Latif[11], C.H. Liu[13], T.C. Liu[5,17], W. Luszczak[2], K. Mase[3], M.S. Muzio[8,9,10], J. Nam[5], R.J. Nichol[7], A. Novikov[15], A. Nozdrina[1], E. Oberla[12], Y. Pan[15], C. Pfendner[18], N. Punsuebsay[15], J. Roth[15], A. Salcedo-Gomez[2], D. Seckel[15], M.F.H. Seikh[1], Y.-S. Shiao[5,19], S.C. Su[5], S. Toscano[20], J. Torres[2], J. Touart[6], N. van Eijndhoven[11], G.S. Varner[21,†], A. Vieregg[12], M.-Z. Wang[5], S.-H. Wang[5], S.A. Wissel[8,9,10], C. Xie[7], S. Yoshida[3], R. Young[1]

[1] Dept. of Physics and Astronomy, University of Kansas, Lawrence, KS 66045
[2] Dept. of Physics, Center for Cosmology and AstroParticle Physics, The Ohio State University, Columbus, OH 43210
[3] Dept. of Physics, Chiba University, Chiba, Japan
[4] Dept. of Physics, University of Wisconsin-Madison, Madison, WI 53706
[5] Dept. of Physics, Grad. Inst. of Astrophys., Leung Center for Cosmology and Particle Astrophysics, National Taiwan University, Taipei, Taiwan
[6] Dept. of Physics, University of Maryland, College Park, MD 20742
[7] Dept. of Physics and Astronomy, University College London, London, United Kingdom
[8] Center for Multi-Messenger Astrophysics, Institute for Gravitation and the Cosmos, Pennsylvania State University, University Park, PA 16802
[9] Dept. of Physics, Pennsylvania State University, University Park, PA 16802
[10] Dept. of Astronomy and Astrophysics, Pennsylvania State University, University Park, PA 16802
[11] Vrije Universiteit Brussel, Brussels, Belgium
[12] Dept. of Physics, Enrico Fermi Institue, Kavli Institute for Cosmological Physics, University of Chicago, Chicago, IL 60637
[13] Dept. of Physics and Astronomy, University of Nebraska, Lincoln, Nebraska 68588
[14] Dept. Physics and Astronomy, Whittier College, Whittier, CA 90602
[15] Dept. of Physics, University of Delaware, Newark, DE 19716
[16] Dept. of Energy Engineering, National United University, Miaoli, Taiwan
[17] Dept. of Applied Physics, National Pingtung University, Pingtung City, Pingtung County 900393, Taiwan
[18] Dept. of Physics and Astronomy, Denison University, Granville, Ohio 43023
[19] National Nano Device Laboratories, Hsinchu 300, Taiwan
[20] Universite Libre de Bruxelles, Science Faculty CP230, B-1050 Brussels, Belgium
[21] Dept. of Physics and Astronomy, University of Hawaii, Manoa, HI 96822
[†] Deceased

PoS(ARENA2024)009

Acknowledgements

The ARA Collaboration is grateful to support from the National Science Foundation through Award 2013134. The ARA Collaboration designed, constructed, and now operates the ARA detectors. We would like to thank IceCube, and specifically the winterovers for the support in operating the detector. Data processing and calibration, Monte Carlo simulations of the detector and of theoretical models and data analyses were performed by a large number of collaboration members, who also discussed and approved the scientific results presented here. We are thankful to Antarctic Support Contractor staff, a Leidos unit for field support and enabling our work on the harshest continent. We thank the National Science Foundation (NSF) Office of Polar Programs and Physics Division for funding support. We further thank the Taiwan National Science Councils Vanguard Program NSC 92-2628-M-002-09 and the Belgian F.R.S.- FNRS Grant 4.4508.01 and FWO. K. Hughes thanks the NSF for support through the Graduate Research Fellowship Program Award DGE-1746045. A. Connolly thanks the NSF for Award 1806923 and 2209588, and also acknowledges the Ohio Supercomputer Center. S. A. Wissel thanks the NSF for support through CAREER Award 2033500. A. Vieregg thanks the Sloan Foundation and the Research Corporation for Science Advancement, the Research Computing Center and the Kavli Institute for Cosmological Physics at the University of Chicago for the resources they provided. R. Nichol thanks the Leverhulme Trust for their support. K.D. de Vries is supported by European Research Council under the European Unions Horizon research and innovation program (grant agreement 763 No 805486). D. Besson, I. Kravchenko, and D. Seckel thank the NSF for support through the IceCube EPSCoR Initiative (Award ID 2019597). M.S. Muzio thanks the NSF for support through the MPS-Ascend Postdoctoral Fellowship under Award 2138121. A. Bishop thanks the Belgian American Education Foundation for their Graduate Fellowship support.